Torque Ripple Reduction in Interior Permanent Magnet Synchronous Machines Using Stators With Odd Number of Slots Per Pole Pair

Seok-Hee Han, *Member, IEEE*, Thomas M. Jahns, *Fellow, IEEE*, Wen L. Soong, *Member, IEEE*, Mustafa K. Güven, *Member, IEEE*, and Mahesh S. Illindala, *Member, IEEE*

***Abstract*—This paper develops analytical principles for torque ripple reduction in interior permanent magnet (IPM) synchronous machines. The significance of slot harmonics and the benefits of stators with odd number of slots per pole pair are highlighted. Based on these valuable analytical insights, this paper proposes coordination of the selection of stators with odd number of slots per pole pair and IPM rotors with multiple layers of flux barriers in order to reduce torque ripple. The effectiveness of using stators with odd number of slots per pole pair in reducing torque ripple is validated by applying a finite-element-based Monte Carlo optimization method to four IPM machine topologies, which are combinations of two stator topologies (even or odd number of slots per pole pair) and two IPM rotor topologies (one- or two-layer). It is demonstrated that the torque ripple can be reduced to less than 5% by selecting a stator with an odd number of slots per pole pair and the IPM rotor with optimized barrier configurations, without using stator/rotor skewing or rotor pole shaping.**

***Index Terms*—Interior permanent magnet (IPM) synchronous machines, odd number of stator slots per pole pair, stator slot harmonics, torque ripple.**

I. Introduction

INTERIOR permanent magnet (IPM) synchronous machines are vulnerable for producing significant amounts of current-induced ripple torque if the machine is not carefully designed to prevent it. For conventional IPM machines, the ratio of the peak-to-peak torque ripple ($T_{\text{p-p}}$) to the average operating torque (T_{avg}) for the rated operation is often approximately 20% at the current angle for maximum torque/ampere operation [1]–[6]. For current angles corresponding to deep flux weakening, the ratio is often above 100% [2], [5].

Reducing torque pulsations in permanent magnet machines has received significant attention in recent years. The two main approaches to pulsating torque reduction are based either on an adequate motor design with intrinsically low pulsating torque for the assumed current waveform or on control techniques, which actively compensate the pulsating torque. Most of the techniques used for reduction of the pulsating torque in PM motors based on motor design and control have been extensively reviewed in [10] and [11]. Although control-based techniques for reduction of pulsating torque in PM motors can be quite effective, the main focus of this paper is design-based approaches for sinusoidal drives.

TABLE I
SUMMARY OF SELECTED LITERATURE ON TORQUE RIPPLE REDUCTION IN PM MACHINES

Ref.	*Machine type*	*Stator slots per pole pair*	*Flux barriers per pole*	*Peak-to-peak torque ripple*
[1]	SynRM	18	3	4.2%
[2]	IPM	18	2	10 %
[3]	IPM	12	1	10 %
[4]	IPM	12	1	23 %
[6]	IPM	12	2	4.6 %
[7]	SPM	9	SPM	3.4%

Table I provides a concise summary of key technical literature on torque ripple reduction, which is more closely related to the approach of this paper. Vagati *et al*. [1] have reduced the $T_{\text{p-p}}$ (at rated torque) of synchronous reluctance machines to values less than 5% by increasing the number of slots per pole pair and the number of flux barriers per pole. Design features such as asymmetric flux barriers [2] or sinusoidal profiling of the rotor surface [3] have been proposed to reduce the $T_{\text{p-p}}$ of IPM machines to values in the vicinity of 10%. Bianchi *et al*. [6] combined two rotor types into a hybrid IPM rotor structure that was then step-skewed to suppress torque ripple to below 5%. Islam *et al*. [7] working on surface PM machines have demonstrated a promising technique for reducing the ripple torque by using a stator winding configuration with an odd number of slots per pole pair.

The objective of this paper is to investigate opportunities for minimizing the ripple torque in IPM machines by coordinating the selection of stators with odd number of slots per pole pair and IPM rotors with multiple layers of flux barriers [8]. First, this paper develops analytical principles for torque ripple estimation in IPM synchronous machines. The significance of slot harmonics and the benefits of stators with odd number of slots per pole pair are highlighted. Based on these valuable analytical insights, this paper proposes coordination of the selection of stators with odd number of slots per pole pair and IPM rotors

Manuscript received December 20, 2008; revised August 5, 2009. First published January 29, 2010; current version published February 17, 2010. This work was supported by Technology and Solutions Division, Caterpillar Inc., Peoria, IL. Paper no. TEC-00508-2008.

S.-H. Han is with the University of Wisconsin, Madison, WI 53706 USA, and also with Caterpillar Inc., Peoria, IL 61629 USA (e-mail: Han_Seok-Hee@cat.com).

T. M. Jahns is with the University of Wisconsin, Madison, WI 53706 USA.

W. L. Soong is with the University of Adelaide, Adelaide, S.A. 5005, Australia.

M. K. Güven and M. S. Illindala are with Caterpillar Inc., Peoria, IL 61629 USA.

Color versions of one or more of the figures in this paper are available online at http://ieeexplore.ieee.org.

Digital Object Identifier 10.1109/TEC.2009.2033196

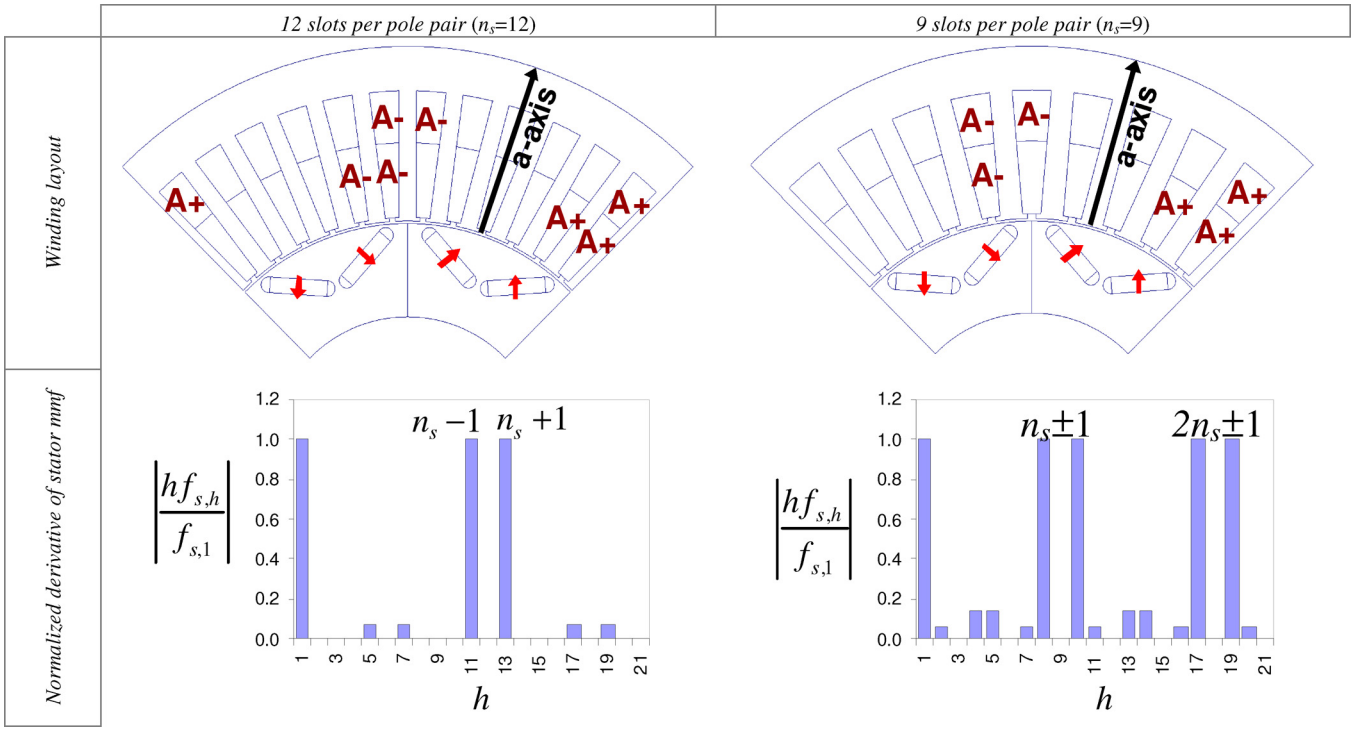

Fig. 1. Stator winding layouts and stator MMF spectra multiplied by the harmonic index h for $n_s = 12$ and $n_s = 9$ cases.

with multiple layers of flux barriers in order to reduce the torque ripple. The effectiveness of stators with odd number of slots per pole pair in reducing torque ripple is validated by applying a finite-element (FE)-based Monte Carlo optimization method to four IPM machine topologies, which are combinations of two stator topologies (even or odd number of slots per pole pair) and two IPM rotor topologies (one- or two-layer). It is demonstrated that the torque ripple can be reduced to less than 5% by coordinating the stator with odd number of slots per pole pair and the IPM rotor with optimized barrier configurations, without stator/rotor skewing or rotor pole shaping.

II. Principles for Torque Ripple Reduction of IPM Machines

This section develops key design principles to reduce torque ripple in IPM machines. Balanced and symmetrical windings are assumed. The impact of imbalances due to manufacturing differences on the torque ripple is neglected. Control-based techniques such as current wave shaping can be quite effective for reduction of pulsating torque in PM motors. However, design-based approaches for sinusoidal drives will be the main focus of this paper.

A. Analytical Index for the Torque Ripple (TPP)

An analytical index TPP reflecting the amplitude of the torque ripple is derived in the Appendix of this paper under the idealized assumptions of no magnetic saturation and closed stator slots as follows:

$$\mathrm{TPP} \equiv \sum_{m=1,2,3,\ldots} |6m \mp 1| \left|\frac{f_{s,6m\mp1}}{f_{s,1}}\right| \left|\frac{f_{r,6m\mp1}}{f_{r,1}}\right| \quad (1)$$

where $f_{s,h}$ and $f_{r,h}$ are hth-order harmonics of the stator MMF f_s and rotor MMF f_r, respectively. This compact expression (1) clearly shows that the torque ripple is the result of the interaction between the stator and rotor MMF harmonics. Although the derived analytic torque ripple index (TPP) neither consider the nonuniform reluctance patterns of the slotted air gap nor the MMF drops across iron core due to saturation, thus, we can draw two key principles from (1).

The first crucial observation drawn from (1) is that each stator MMF harmonic $f_{s,h}$ is amplified by the harmonic order h, interacts with the corresponding rotor MMF harmonic of the same harmonic order, and produces torque ripple. Mathematically, multiplication by the harmonic order in the frequency domain ($hf_{s,h}$) is equivalent to differentiation in the spatial domain (df_s). Recall that the stator MMF f_s can be interpreted to be the spatial accumulation (i.e., integral) of the stator ampere-turn distribution measured from a selected reference location, and hence, the spatial differential df_s of the stator MMF corresponds to the stator ampere-turn distribution along the periphery of the stator bore. As a result, it can be restated that the interaction between the derivative of the stator MMF, i.e., stator ampere-turn distribution, and the rotor MMF produces torque ripple. As noted earlier, the differentiation operation causes each stator MMF harmonic $f_{s,h}$ to be amplified by its harmonic order h. Thus, higher order MMF harmonic components can disproportionately contribute to the torque ripple amplitude. Since the stator and rotor MMF waveforms have step discontinuities caused by the stator slotting and flux barriers, special attention must be devoted to the discontinuities because of the high-frequency harmonics that they can create.

TABLE II
IPM MACHINE SPECIFICATIONS

Rated torque	600 Nm
Rated line-to-line voltage	612 Vpk
Rated phase current	168 Apk
Base speed	875 rpm
Maximum speed	8224 rpm
Back-emf at base speed	273 Vllpk
Characteristic current	104 Apk
Poles	8
Stator OD	281.6 mm
Rotor OD	160.3 mm
Active stack length	321.5 mm
PM remanent flux density at 150°C	0.974 T

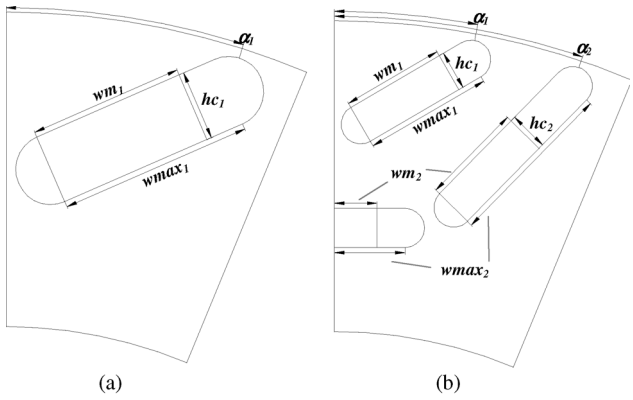

Fig. 2. Geometrical parameters for one- and two-layer IPM rotors. (a) One-layer rotor. (b) Two-layer rotor.

The second crucial observation drawn from (1) is that only stator and rotor MMF harmonics with orders of $6m \pm 1$ contribute to the torque ripple with orders of $6m$. This results from the fact that the stator MMF does not have triple harmonics due to the floating star connection and the rotor MMF has only odd-numbered harmonics due to the geometrical symmetry. Since $6m \pm 1$ are odd numbers, it can be concluded that even-ordered harmonics do not contribute to torque ripple.

In summary, two crucial principles are drawn from (1).

1) Each stator MMF harmonic $f_{s,h}$ is amplified by the harmonic order h.
2) Even-ordered harmonics do not contribute to torque ripple.

As will be shown in Section II-B, the first design principle highlights the significance of slot harmonics and the second highlights the benefits of stators with odd number of slots per pole pair.

B. Stator Winding Configurations With Even Versus Odd Number of Slots per Pole Pair

This paper compares two classes of distributed stator winding configurations: 1) one with even number of slots per pole pair; and 2) the other with odd number of slots per pole pair. It is shown that stator windings with odd number of slots per pole pair are advantageous in reducing mutual interactions between

TABLE III
RANGES OF RANDOM VARIATIONS FOR ROTOR GEOMETRICAL PARAMETERS

	One-layer rotor	Two-layer rotor
α_1	60°~75°	30°~45°
α_2	-	60°~75°
hc_1/g_p	6~9	3~6
hc_2/g_p	-	3~6
$wm_1/wmax_1$	0.8~1	1
$wm_2/wmax_2$	-	0.9
number of iterations	5^3=125	5^4=625

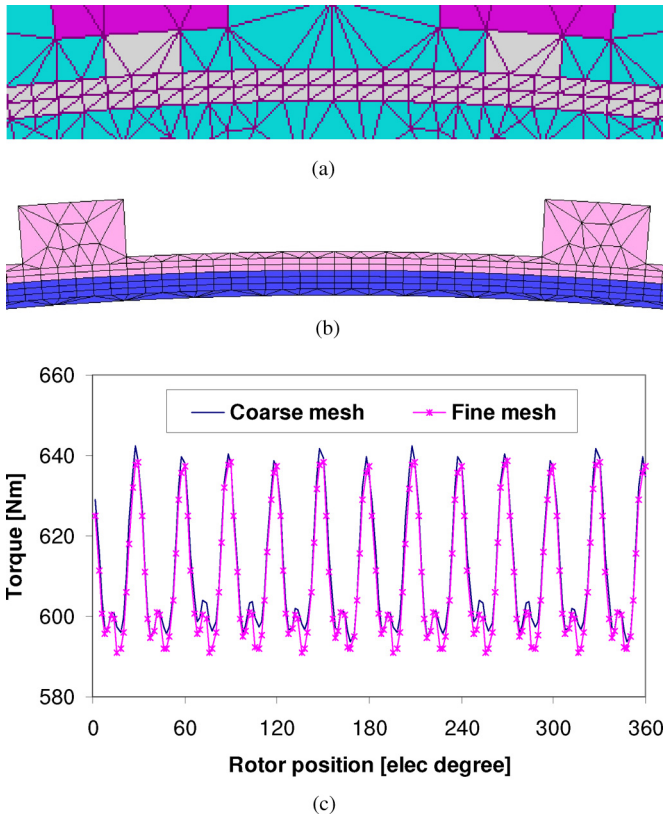

Fig. 3. FE mesh in the air gap for torque calculation. (a) Coarse mesh in the air gap. (b) Fine mesh in the air gap. (c) Torque waveforms computed with coarse and fine meshes in the air gap.

the stator and rotor MMF harmonics. We will denote the number of stator slots per pole pair by n_s [1], [8]. In addition, we will name the harmonics with orders of $kn_s \pm 1$, where $k = 1, 2, 3, \ldots$, as the stator slot harmonics.

Fig. 1 illustrates two typical distributed stator winding configurations: one with $n_s = 12$ in the left column and the other with $n_s = 9$ in the right column. The first row shows their winding layouts. The second row shows the spectral components of the normalized derivatives of their stator MMF distributions. The detailed algebraic derivation will be given in the Appendix.

The harmonic order multiplication has the effect of amplifying the slot harmonics ($h = kn_s \pm 1$) so that their amplitudes match that of the fundamental component, regardless of whether n_s is even or odd. This observation suggests that the stator slot harmonics are particularly potent components for contributing to the ripple torque. Therefore, for low torque ripple design, the

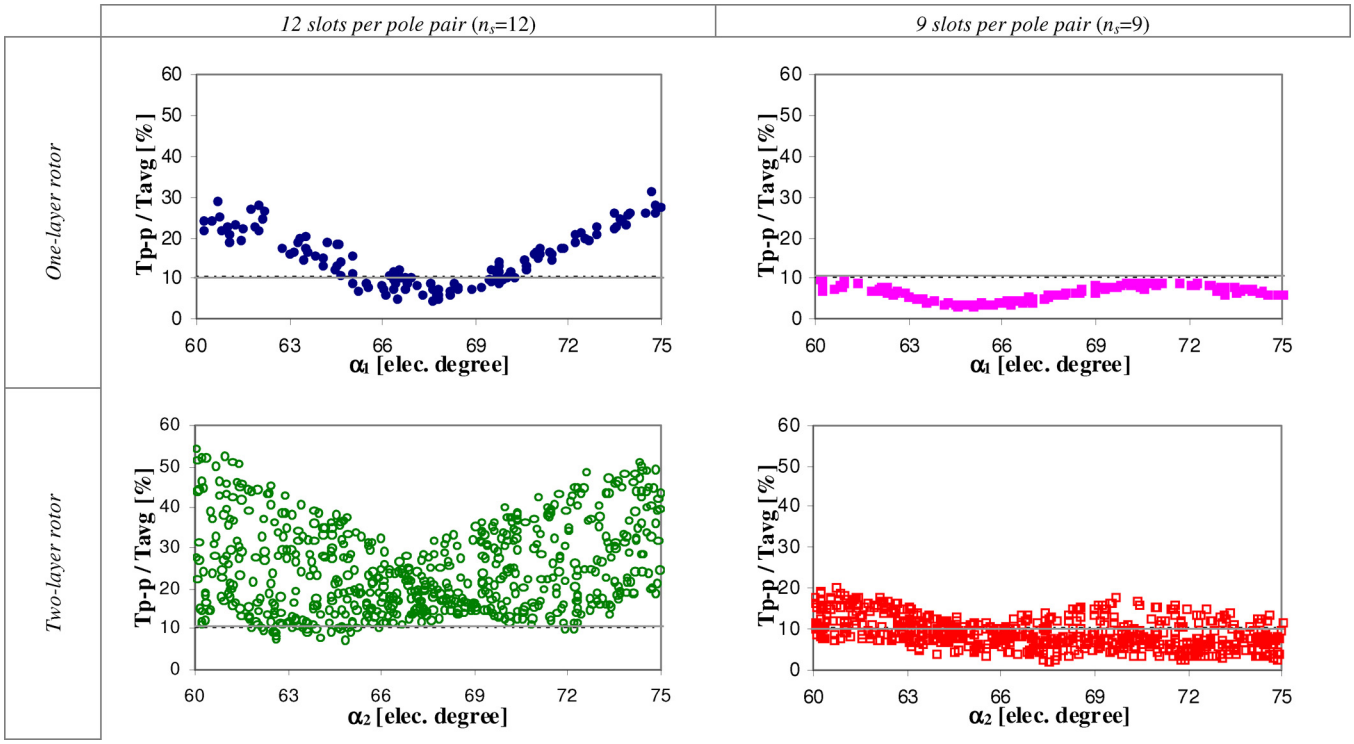

Fig. 4. Scatter plots of FE calculated torque ripple versus the barrier-end angle at the rated operation for the four machine topologies for the 125 one-layer designs and 625 two-layer designs.

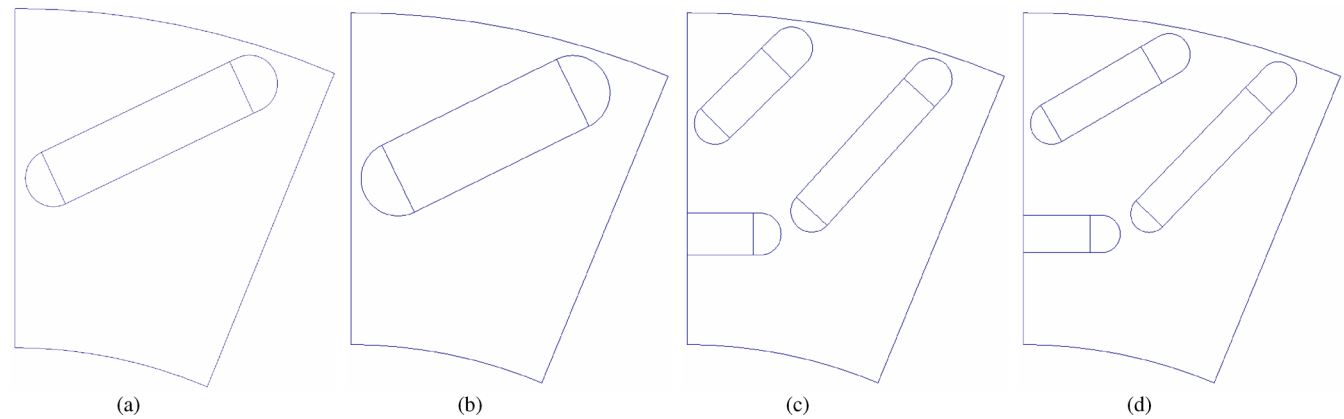

Fig. 5. Cross sections of the rotors for the four representative IPM designs. (a) I-12-TPP. (b) I-9-TPP. (c) II-12-TPP. (d) II-9-TPP.

rotor harmonics of orders $h = kn_s \pm 1$ should be minimized so that interactions between the rotor harmonics and the stator slot harmonics can be minimized.

Now, if n_s is even-numbered, all of the stator slot harmonics ($h = kn_s \pm 1$) are odd-numbered. For example, the set of slot harmonic orders for the case of $n_s = 12$ includes 12 ± 1, 24 ± 1, and so on, all of which are odd-numbered. As the rotor MMF only has odd-numbered harmonics, there is thus a major opportunity for undesirable interactions between the stator and rotor MMF harmonic components that produce ripple torque. However, if n_s is odd-numbered, half of the stator slot harmonics ($h = kn_s \pm 1$) are even-numbered, which do not contribute to torque ripple. For example, the set of slot harmonic orders for the case of $n_s = 9$ includes 9 ± 1, 18 ± 1, and so on. Among these orders, one-half (e.g., 9 ± 1) are even-numbered, while the other-half (e.g., 18 ± 1) are odd-numbered. Consequently, half of the stator slot harmonics cannot interact to produce ripple torque with the rotor MMF harmonics that are all odd-numbered.

In summary, stators with odd number of slots per pole pair reduce the interactions between the rotor MMF and the stator slot harmonics by 50% compared to stators with even number of slots per pole pair. Therefore, adoption of stators with odd number of slots per pole pair can significantly reduce the ripple torque [7], [8].

III. Finite-Element (FE) Monte Carlo Optimization

Since the derived analytic TPP does not consider the nonuniform reluctance patterns of the slotted air gap and the MMF

TABLE IV
GEOMETRICAL PARAMETERS OF THE ROTORS FOR THE FOUR REPRESENTATIVE IPM DESIGNS

	I-12-TPP	I-9-TPP	II-12-TPP	II-9-TPP
α_1	68.5°	66°	30°	42°
α_2	-	-	71°	74°
hc_1	5.37 mm	7.16 mm	4.03 mm	4.03 mm
hc_2	-	-	4.03 mm	3.58 mm
wm_1	20.0 mm	18.8 mm	8.29 mm	11.2 mm
wm_2	-	-	21.8 mm	21.7 mm

drops across the iron core due to saturation, this section uses a FE-based torque calculation method to validate the effectiveness of stators with odd number of slots per pole pair in reducing torque ripple of IPM machines. A FE-based Monte Carlo optimization that is basically a random search method is applied to four machine topologies. These are combinations of two rotor topologies (one- or two-layer) and two stator topologies ($n_s = 12$ or 9 slots per pole pair). They are named as I-12, I-9, II-12, and II-9, respectively, where the first Roman number (I or II) stands for the number of rotor layers, while the second Arabic number (12 or 9) denotes the number of stator slots per pole pair.

Two stators (one with $n_s = 12$ and the other with $n_s = 9$) are predesigned according to the IPM machine specification in Table II. Their cross sections are shown in Fig. 1. The geometrical parameters for the rotor are randomly changed. The geometrical design parameters for the one- and two-layer IPM rotors are defined in Fig. 2. The selected ranges of the variations for the rotor geometrical parameters are summarized in Table III. All three geometrical parameters for one-layer rotor (α_1, hc_1, and wm_1) are randomly varied. For two-layer rotor, out of total six geometrical parameters ($\alpha_1, \alpha_2, hc_1, hc_2, wm_1$, and wm_2), the four geometrical parameters (α_1, α_2, hc_1, and hc_2) are randomly varied, while the two geometrical parameters (wm_1 and wm_2) remain fixed. The number of random designs tested are $5^3 = 125$ and $5^4 = 625$ for the one- and two-layer rotors, respectively.

For each design, the torque waveform calculated by the FE Maxwell stress vector is recorded for the rotor motion through 60° electrical (one phase belt) in steps of 2° electrical under the rated current excitation ($i_m = 168\ \mathrm{A_{pk}}$ and current angle $\gamma_d = 50°$ electrical). Fig. 3 shows the two FE meshes in the air gap for the torque calculations. In Fig. 3(a), the air gap is meshed in two layers in the radial direction and in one division per 2° electrical in the circumferential direction. In Fig. 3(b), the air gap is meshed in seven layers in the radial direction and in one division per 1° electrical in the circumferential direction. In Fig. 3(c), the torque waveforms for the same representative design calculated with two different meshes shown in Fig. 3(a) and (b) are compared. They are close enough. The coarse mesh in Fig. 3(a) is used to save computation time.

The scatter plots of the FE calculated torque ripple versus the angular air gap position of one of the rotor barrier ends under rated operation are shown in Fig. 4 for the 125 one-layer designs and the 625 two-layer designs. The torque ripple is defined as the ratio of the $T_{\text{p-p}}$ to the T_{avg}. For the I-12 topology, the torque ripple can be as low as 5%. The optimal barrier-end angle to give the minimum torque ripple is 67.5°. The torque ripple remains below 10% for barrier-end angles from 64° to 70°. The torque ripple can be as high as 30% for barrier-end angles away from the optimal angle in either direction. For the I-9 topology, the torque ripple can be as low as 3%. The optimal barrier-end angle to give the minimum torque ripple is around 65°. It is impressive to see that the torque ripple remains below 10% for the full range of barrier-end angles from 60° to 75°. For the II-12 topology, surprisingly, few designs have a torque ripple below 10%. Instead, the torque ripple can easily exceed 30% for all outer barrier-end α_2 values between 60° and 75°, respectively. For the II-9 topology, the maximum torque ripple is about 20%. There are many designs with torque ripple below 10%. The torque ripple can be as low as 3%.

Major conclusions are given in the following points.

1) The I-9 and II-9 topologies are shown to have much lower torque ripple for a wider domain of design space than I-12 and II-12 topologies, respectively. This means that nine slots per pole pair designs can be optimized for other machine performance criteria, while keeping torque ripple low. This also means that torque ripple of nine slots per pole pair designs is less sensitive to manufacturing variations.
2) Two-layer rotors can have higher torque ripple than one-layer rotors. It has been shown that the II-12 and II-9 topologies can have higher torque ripples than I-12 and I-9 topologies, respectively.

IV. TORQUE RIPPLE SPECTRAL ANALYSIS

This section presents the spectral analysis of the torque waveforms for four representative designs from the four machine topologies. Each of the four representative designs has been selected from the corresponding pool of the random designs and adjusted further such that: 1) the torque ripple should remain close to the minimum value and 2) the PM flux linkage, the characteristic current, and the rated average torque should be close to the specified values in Table II. The four representative designs are named I-12-TPP, I-9-TPP, II-12-TPP, and II-9-TPP, respectively.

The cross sections and geometrical parameters of the rotors for the four representative designs are shown in Fig. 5 and Table IV. The PM flux linkage, the characteristic current, and the rated average torque of the four designs are compared in Table V and are shown to be similar. Thus, all four designs have approximately the same basic performance characteristics, although their predicted torque ripple amplitudes differ.

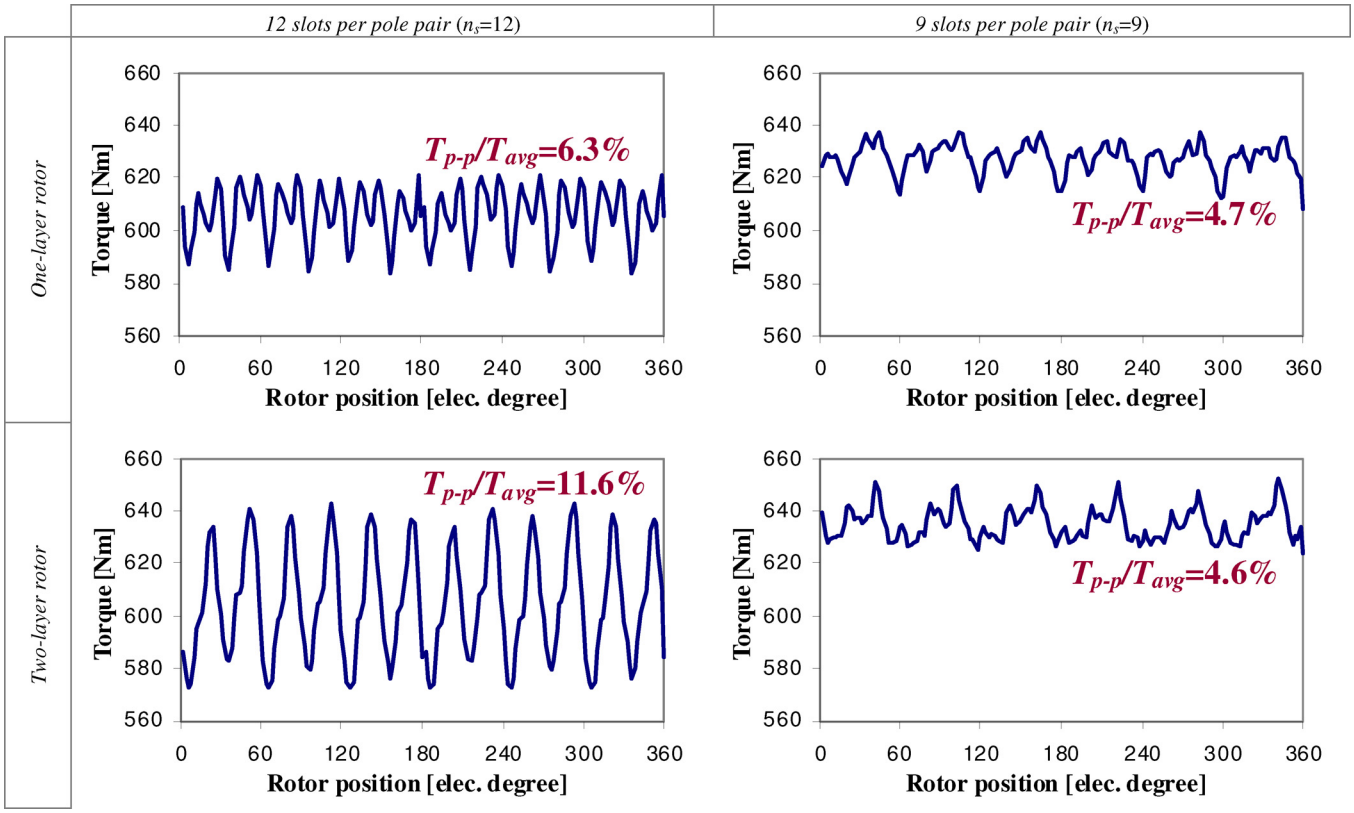

Fig. 6. Torque waveforms for the four representative IPM designs at the rated operation (at 875 r/min with 168 A_{pk} at a current angle of 50° electrical from the positive *q*-axis).

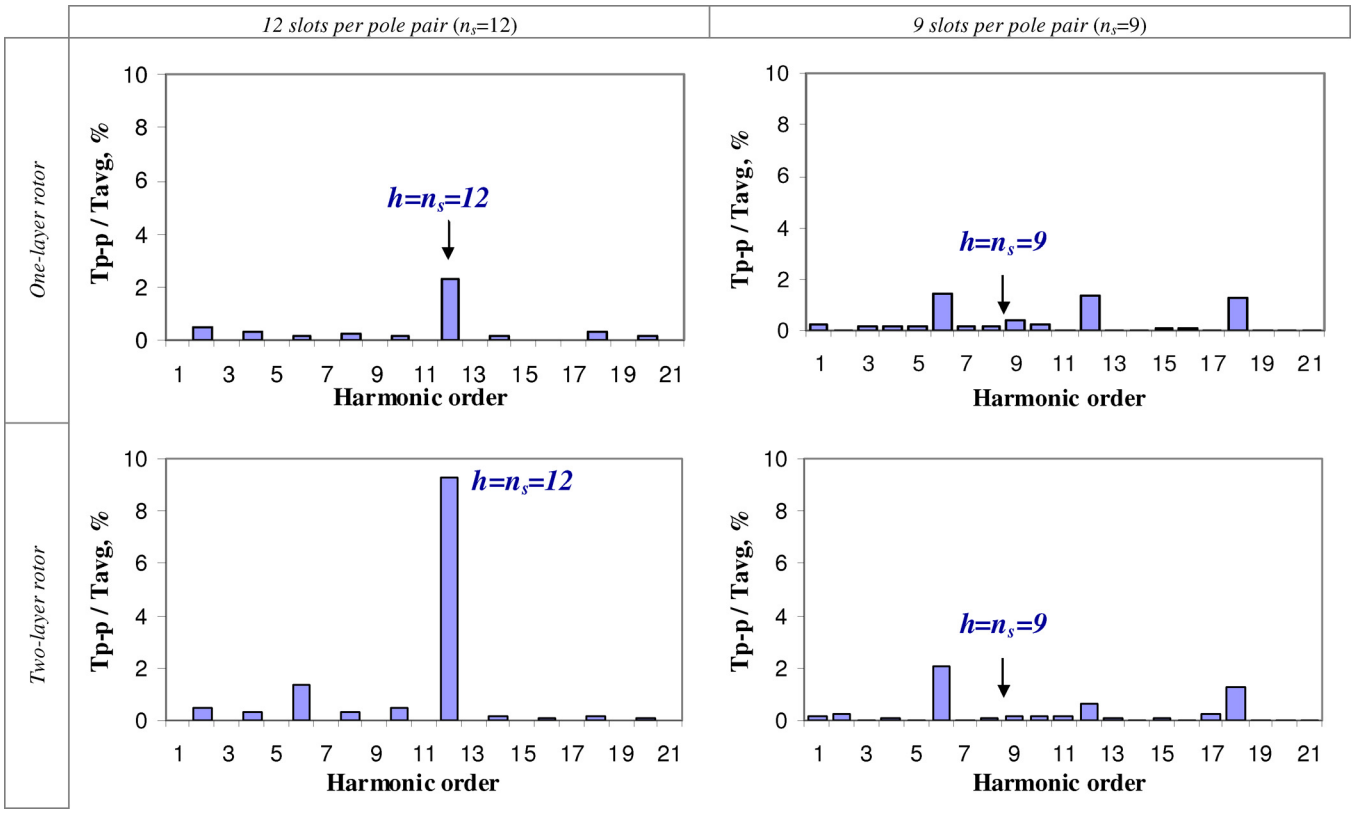

Fig. 7. Spectrum of torque waveforms for the four-representative IPM designs at the rated operation (at 875 r/min with 168 A_{pk} at a current angle of 50° electrical from the positive *q*-axis).

TABLE V
FE CALCULATED BASIC PERFORMANCE PARAMETERS AND TORQUE RIPPLE FOR THE FOUR REPRESENTATIVE IPM DESIGNS

	I-12-TPP	*I-9-TPP*	*II-12-TPP*	*II-9-TPP*
PM flux linkage	0.4344 [Vpk-sec]	0.4328 [Vpk-sec]	0.4299 [Vpk-sec]	0.4333 [Vpk-sec]
Characteristic current	102.6 [Apk]	103.7 [Apk]	102.2 [Apk]	104 [Apk]
Rated average torque	607 [Nm]	628 [Nm]	605 [Nm]	635 [Nm]
Torque ripple amplitude	6.3%	4.7%	11.6%	4.6%
Harmonic frequency	12^{th}	6^{th}	12^{th}	6^{th}

The torque waveforms and corresponding spectra at rated current for the four representative designs are shown in Figs. 6 and 7. It can be observed from the spectral analysis in Fig. 7 that: 1) for $n_s = 12$, the torque ripple harmonic component at the order of $h = n_s$ is dominant and 2) for $n_s = 9$, the torque ripple harmonic component at the order of $h = n_s$ does not exist. These results support the principles in Section II that the first dominant slot harmonics appearing at $h = n_s \pm 1$ for $n_s = 9$ have even order numbers and does not interact with the rotor MMF harmonics to produce ripple torque. As a result, stators with $n_s = 9$ are more effective than stators with $n_s = 12$ for reducing the torque ripple amplitude though the torque ripple frequency is halved.

An extensive discussion on other potential trade-offs that are anticipated when using odd versus even number stator slots can be found in [13] and [14]. The effects on rotor eddy-current losses when the stator slots and rotor layers vary are investigated in [13]. The design trade-off between torque ripple and stator core losses when the stator slots and rotor layers vary is examined in [14].

V. CONCLUSION

This paper has developed analytical insights for torque ripple reduction in IPM synchronous machines. The impact of the stator–rotor harmonic interactions on the torque ripple has been clearly highlighted, providing helpful insights into potential design improvements. The significance of the slot harmonics and the benefits of stators with odd number of slots per pole pair have been emphasized. Based on these valuable analytical insights, this paper has examined using stators with odd number of slots per pole pair and IPM rotors with multiple layers of flux barriers in order to reduce the torque ripple.

To validate the effectiveness of stators with odd number of slots per pole pair in reducing torque ripple, a FE-based Monte Carlo optimization method has been applied to four machine topologies, which are combinations of two stator topologies (even or odd number of slots per pole pair) and two rotor topologies (one- or two-layer). It has been demonstrated that torque ripple can be reduced to less than 5% by using a stator with an odd number of slots per pole pair and an IPM rotor with optimized barrier configurations, without using stator/rotor skewing or rotor pole shaping.

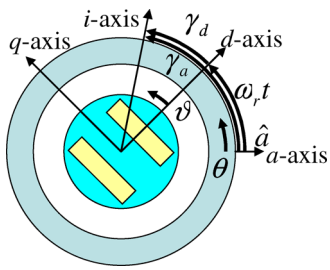

Fig. 8. Definitions of key axes, current control angles, rotor position angle, and spatial coordinates in stator and rotor reference frames.

APPENDIX

This section derives the analytical expression for the instantaneous IPM torque ripple under the idealized assumptions of no magnetic saturation and closed stator slots. The stator conductors are modeled by a current sheet along the air gap surface. Compared to the existing expressions available in the literature [1] and [6], the usefulness of the torque ripple expression developed in this paper is that it clearly highlights the impact of the stator–rotor harmonic interactions on the torque ripple, providing helpful insights into potential design improvements. The key axes, angles of the current excitation and the rotor position, and the spatial coordinates in the stator and rotor reference frames are illustrated in Fig. 8.

A. Winding Function

The winding function n of the stator phase winding is defined as the spatial accumulation (i.e., integral) of the conductor distribution for one stator phase measured from a selected reference location [9]. Fig. 9 shows the winding functions for the winding layouts introduced in Fig. 1.

The winding function can be expanded into its Fourier series as follows:

$$n = \sum_{h=1,2,3,\ldots} n_h \cos(h\theta) \tag{2}$$

where h is the harmonic index, n_h is the hth-order stator winding harmonic, and θ is the angular position (electrical radian) in the stator reference frame measured from the phase a-axis. It is assumed that the winding function is even symmetric about the phase a-axis and that the winding functions of phases b and c are identical but displaced by $2\pi/3$ and $4\pi/3$ electrical radian, respectively. The spectral components for the example winding functions in Fig. 8 are given by

$$n_h = \begin{cases} \dfrac{1}{\pi h}\left[\sin\left(\dfrac{60\pi h}{180}\right) + 2\sin\left(\dfrac{90\pi h}{180}\right) + \sin\left(\dfrac{120\pi h}{180}\right)\right] & n_s = 12 \\ \dfrac{4}{3\pi h}\left[\sin\left(\dfrac{60\pi h}{180}\right) + 2\sin\left(\dfrac{100\pi h}{180}\right)\right] & n_s = 9. \end{cases}$$

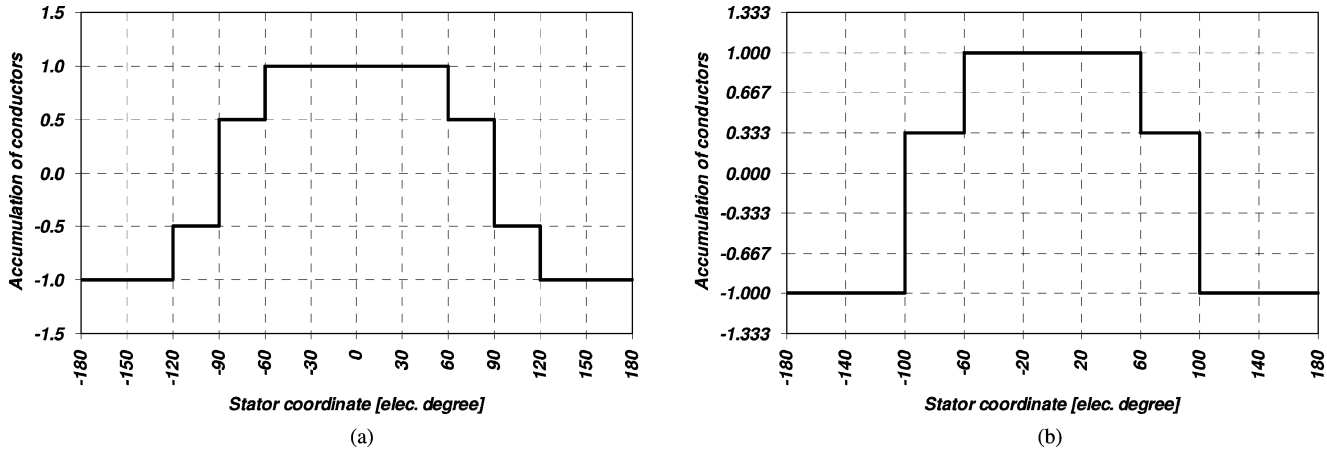

Fig. 9. Winding functions for the winding layouts introduced in Fig. 1. (a) Twelve slots per pole pair ($n_s = 12$). (b) Nine slots per pole pair ($n_s = 9$).

B. Stator MMF

For a given set of instantaneous phase currents (i_a, i_b, and i_c), the stator MMF f_s has the instantaneous spatial distribution given by

$$f_s = n(\theta)i_a + n(\theta - 120^\circ)i_b + n(\theta - 240^\circ)i_c. \tag{3}$$

Note that the stator MMF f_s can be interpreted to be the spatial accumulation (i.e., integral) of the stator ampere-turn distribution measured from a selected reference location.

The phase current excitation can be expressed by an instantaneous current vector in the stator reference frame as

$$i_a\hat{a} + i_b\hat{b} + i_c\hat{c} \equiv \frac{3}{2}i_m \angle\gamma_a \tag{4}$$

where $\hat{a}$, $\hat{b}$, and $\hat{c}$ are unit vectors along the a-axis, b-axis, and c-axis, respectively, i_m is the current vector amplitude, and γ_a is the current vector angle measured from the a-axis (see Fig. 8). It is assumed that the three phases windings are connected in a floating star configuration so that the three instantaneous phase currents always sum to zero

$$i_a + i_b + i_c = 0. \tag{5}$$

Combining (4) and (5) yields

$$\begin{aligned} i_a &= i_m \cos(\gamma_a) \\ i_b &= i_m \cos(\gamma_a - 2\pi/3) \\ i_c &= i_m \cos(\gamma_a - 4\pi/3). \end{aligned}$$

Next, the Fourier series expansion of f_s can be expressed as

$$\begin{aligned} f_s = &\sum_{h=1,4,7,\ldots} 1.5n_h i_m \cos(h\theta - \gamma_a) \\ &+ \sum_{h=2,5,8,\ldots} 1.5n_h i_m \cos(h\theta + \gamma_a) \\ &+ \sum_{h=3,6,9,\ldots} 0. \end{aligned} \tag{6}$$

Introducing $f_{s,h}$ as the notation for the hth-order stator MMF harmonic, it can be seen that the stator MMF is related to the winding function as follows:

$$f_{s,h} = \begin{cases} 1.5n_h i_m, & h \neq 3, 6, 9, \ldots \\ 0, & h = 3, 6, 9, \ldots \end{cases}.$$

Transforming the stator MMF into the rotor reference frame yields

$$f_s = \sum_{h\neq 3,6,9,\ldots} f_{s,h} \cos(h\theta \mp \omega_r t \mp \gamma_d) \tag{7}$$

where $\omega_r t$ is the instantaneous rotor angular position and γ_d is the current phase angle measured from the d-axis. The spatial derivative of f_s can be computed to be

$$\frac{df_s}{d\theta} = -\sum_{h\neq 3,6,9,\ldots} h f_{s,h} \sin(h\theta \mp \omega_r t \mp \gamma_d). \tag{8}$$

Fig. 1 illustrates the spectral components of the normalized derivatives of the stator MMF distributions for the two example winding layouts under consideration.

C. Rotor MMF

In response to any given set of instantaneous phase current excitation values (i_a, i_b, and i_c), the presence of flux barriers inside the IPM rotor induces an instantaneous spatial distribution of rotor MMF f_r, which can be expanded into a Fourier series

$$f_r = \sum_{h\neq 2,4,\ldots} f_{r,h} \cos(h\vartheta) \tag{9}$$

where $f_{r,h}$ is the hth-order rotor MMF harmonic and ϑ is the angular spatial coordinate [electrical radian] in the rotor reference frame (see Fig. 8). The rotor MMF is even symmetric about the d-axis and odd symmetric about the q-axis. Therefore, it has no even harmonics. Transforming the rotor MMF into the stator reference frame yields

$$f_r = \sum_{h\neq 2,4,\ldots} f_{r,h} \cos(h\theta - h\omega_r t). \tag{10}$$

D. Torque Ripple

Application of the Lorentz force law along the air gap surface leads to an expression for the instantaneous torque T_e

$$\begin{aligned} T_e &= r_g l_{\rm stk} \int_{2\pi\times\frac{P}{2}} B_g df_s \\ &= \frac{P}{2}\frac{\mu_0}{g} r_g l_{\rm stk} \int_{2\pi} (f_r - f_s)\frac{df_s}{d\theta} d\theta \qquad \text{[N·m]} \\ &= \frac{P}{2}\frac{\mu_0}{g} r_g l_{\rm stk} \left\{ \int_{2\pi} f_r \frac{df_s}{d\theta} d\theta - \int_{2\pi} f_s \frac{df_s}{d\theta} d\theta \right\} \quad (11) \end{aligned}$$

where r_g is the air gap radius, $l_{\rm stk}$ is the active stack length, P is the number of poles, B_g is the air gap flux density, and μ_0 is the permeability of the air. It follows from the machine periodicity that

$$\int_{2\pi} f_s \frac{df_s}{d\theta} d\theta = \left[\frac{1}{2} f_s^2(\theta)\right]_0^{2\pi} = 0. \quad (12)$$

On the other hand, substitution of the Fourier expansions for f_s and f_r leads to

$$\int_{2\pi} \left(-\frac{df_s}{d\theta}\right) f_r d\theta = \sum_{h=1,5,7,\ldots} \{\pi h f_{s,h} f_{r,h} \sin((h\mp 1)\omega_e t \mp \gamma_d)\}. \quad (13)$$

Separating the fundamental and harmonic components yields

$$\begin{aligned} \int_{2\pi} \left(-\frac{df_s}{d\theta}\right) f_r d\theta &= \pi f_{s,1} f_{r,1} \sin(-\gamma_d) \\ &+ \sum_{\substack{h=6m\mp 1 \\ m=1,2,3,\ldots}} \{\pi h f_{s,h} f_{r,h} \sin((h\pm 1)\omega_e t \pm \gamma_d)\}. \quad (14) \end{aligned}$$

Therefore, we can define the average torque T_1 by

$$T_1 = \frac{P}{2}\frac{\mu_0}{g} r_g l_{\rm stk} \pi f_{s,1} f_{r,1} \sin(\gamma_d) \quad (15)$$

and the ripple torque $T_{\rm ripple}$ by

$$\begin{aligned} T_{\rm ripple} &= -\frac{P}{2}\frac{\mu_0}{g} r_g l_{\rm stk} \pi \\ &\times \sum_{\substack{h=6m\mp 1 \\ m=1,2,3,\ldots}} (h f_{s,h} f_{r,h} \sin((h\pm 1)\omega_e t \pm \gamma_d)). \end{aligned} \quad (16)$$

It should be noted in this equation that the negative sign in the h index of the summation (i.e., $h = 6m - 1$) maps into the two positive signs in the argument of the trigonometric expression (i.e., $(h+1)\omega_e t + \gamma_d$), and *vice versa*.

Using (15) and (16), the ratio of the ripple torque to the average torque is

$$\begin{aligned} \frac{T_{\rm ripple}}{T_1} &= -\frac{1}{\sin(\gamma_d)} \\ &\times \sum_{\substack{h=6m\mp 1 \\ m=1,2,3,\ldots}} \left(h\left(\frac{f_{s,h}}{f_{s,1}}\right)\left(\frac{f_{r,h}}{f_{r,1}}\right) \sin((h\pm 1)\omega_e t \pm \gamma_d)\right). \end{aligned} \quad (17)$$

This compact expression clearly shows that the torque ripple is the result of the interaction between the stator and rotor MMF harmonics. Based on this formulation, the TPP is defined as follows:

$$\text{TPP} \equiv \sum_{\substack{h=6m\pm 1 \\ m=1,2,3,\ldots}} h\left(\frac{f_{s,h}}{f_{s,1}}\right)\left(\frac{f_{r,h}}{f_{r,1}}\right). \quad (18)$$

ACKNOWLEDGMENT

The authors would like to thank the Wisconsin Electric Machines and Power Electronics Consortium for use of its facilities.

REFERENCES

[1] A. Vagati, M. Pastorelli, G. Franceschini, and S. C. Petrache, "Design of low-torque-ripple synchronous reluctance motors," *IEEE Trans. Ind. Appl.*, vol. 34, no. 4, pp. 758–765, Jul./Aug. 1998.

[2] M. Sanada, K. Hiramoto, S. Morimoto, and Y. Takeda, "Torque ripple improvement for synchronous reluctance motor using an asymmetric flux barrier arrangement," *IEEE Trans. Ind. Appl.*, vol. 40, no. 4, pp. 1076–1082, Jul./Aug. 2004.

[3] D. M. Ionel, M. Popescu, M. I. McGilp, T. J. E. Miller, and S. J. Dellinger, "Assessment of torque components in brushless permanent-magnet machines through numerical analysis of the electromagnetic field," *IEEE Trans. Ind. Appl.*, vol. 41, no. 5, pp. 1149–1158, Oct. 2005.

[4] S.-I. Kim, J.-Y. Lee, Y.-K. Kim, J.-P. Hong, Y. Hur, and Y.-H. Jung, "Optimization for reduction of torque ripple in interior permanent magnet motor by using the Taguchi method," *IEEE Trans. Magn*, vol. 41, no. 5, pp. 1796–1799, May 2005.

[5] S.-I. Kim, J.-H. Bhan, J.-P. Hong, and K.-C. Lim, "Optimization technique for improving torque performance of concentrated winding interior PM synchronous motor with wide speed range," in *Proc. 2006 IEEE Ind. Appl. Soc. Annu. Meet.*, pp. 1933–1940.

[6] N. Bianchi, S. Bolognani, D. Bon, and M. Dai Pre, "Rotor flux-barrier design for torque ripple reduction in synchronous reluctance motors," in *Proc. 2006 IEEE Ind. Appl. Soc. Annu. Meet.*, pp. 1193–1200.

[7] M. S. Islam, S. Mir, T. Sebastian, and S. Underwood, "Design considerations of sinusoidally excited permanent-magnet machines for low-torque-ripple applications," *IEEE Trans. Ind. Appl.*, vol. 41, no. 4, pp. 955–962, Jul./Aug. 2005.

[8] S.-H. Han, T. M. Jahns, and W. L. Soong, "Torque ripple reduction in interior permanent magnet synchronous machines using the principle of mutual harmonics exclusion," in *Proc. 2007 IEEE Ind. Appl. Soc. Annu. Meet*, pp. 558–565.

[9] D. W. Novotny and T. A. Lipo, *Vector Control and Dynamics of AC Drives*. Oxford, U.K.: Clarendon, 1998.

[10] T. M. Jahns and W. L. Soong, "Pulsating torque minimization techniques for permanent magnet AC motor drives–a review," *IEEE Trans. Ind. Elec.*, vol. 43, no. 2, pp. 321–330, Apr. 1996.

[11] D. Zarko, "A systematic approach to optimized design of permanent magnet motors with reduced torque pulsations," Ph.D. thesis, Dept. Elect. Comp. Eng., UW-Madison, Madison, WI, 2004.

[12] E. C. Lovelace, "Optimization of a magnetically saturable interior PM synchronous machine drive," Ph.D. thesis, Dept. Elect. Eng. Comput. Sci., Massachusetts Inst. Technol., Cambridge, MA, 2000.

[13] S.-H. Han, T. M. Jahns, and Z. Q. Zhu, "Analysis of rotor core eddy-current losses in interior permanent magnet synchronous machines," in *Proc. 2008 IEEE Ind. Appl. Soc. Annu. Meet.*, pp. 1–8.

[14] S.-H. Han, T. M. Jahns, and Z. Q. Zhu, "Design tradeoffs between stator core loss and torque ripple in IPM machines," in *Proc. 2008 IEEE Ind. Appl. Soc. Annu. Meet.*, 2010, pp. 1–8.

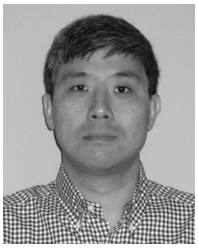

Seok-Hee Han (M'07) was born in Seoul, Korea. He received the B.S., M.S., and Ph.D. degrees in control and instrumentation engineering from Seoul National University, Seoul, Korea, in 1989, 1991, and 1995, respectively. He is currently working toward the Ph.D. degree in electrical and computer engineering from the University of Wisconsin, Madison.

From 1995 to 2000, he was with Samsung Electronics, Gyeonggi, Korea. Since 2008, he has been with Caterpillar Inc., Peoria, IL. His current research interests include high-performance electric machines and drives.

Thomas M. Jahns (S'73–M'79–SM'91–F'93) received the S.B. and S.M., and Ph.D. degrees in electrical engineering from the Massachusetts Institute of Technology, Cambridge, in 1974 and 1978, respectively.

In 1998, he joined as a Grainger Professor of Power Electronics and Electric Machines with the Department of Electrical and Computer Engineering, University of Wisconsin (UW), Madison, where he is currently a Co-Director of the Wisconsin Electric Machines and Power Electronics Consortium. Before joining UW, he was with GE Corporate Research and Development (now GE Global Research Center), Niskayuna, NY, for 15 years, where he was engaged on the new power electronics and motor drive technology in a variety of research and management positions. His research interests include high-performance permanent-magnet synchronous machines and distributed electric resources, including microgrids. From 1996 to 1998, he conducted a research sabbatical at the Massachusetts Institute of Technology, where he directed research activities in the area of advanced automotive electrical systems and accessories as Co-Director of an industry-sponsored automotive consortium.

Dr. Jahns received the 2005 IEEE Nikola Tesla Award. He was awarded the William E. Newell Award by the IEEE Power Electronics Society, in 1999. He has been recognized as a Distinguished Lecturer by the IEEE Industry Applications Society during 1994–1995 and by IEEE-PELS during 1998–1999. He has served as President of PELS (1995–1996) and as Division II Director on the IEEE Board of Directors (2001–2002).

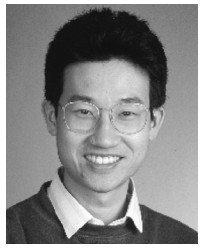

Wen L. Soong (S'89–M'93) was born in Kuala Lumpur, Malaysia. He received the B.Eng. degree from the University of Adelaide, Adelaide, S.A., Australia, in 1989, and the Ph.D. degree from the University of Glasgow, Scotland, U.K., in 1993.

For four years, he was engaged as an Electrical Engineer in the Power Controls Program, General Electric Corporate Research and Development, Schenectady, New York, before joining the Electrical and Electronic Engineering Department, University of Adelaide, in 1998. He is currently with the University of Adelaide, Adelaide. His research interests include permanent magnet and reluctance machines, renewable energy generation, and condition monitoring and diagnostics.

Mustafa K. Güven (M'01) received the B.Sc. degree in electrical engineering from Istanbul Technical University, Istanbul, Turkey, in 1993, specializing on in micro processor-based industrial system, and the M.S. and Ph.D. degrees in electrical engineering from the Ohio State University, Columbus, in 1997 and 2001, respectively, specializing in control system theory and in power electronics, electric machines and drives, respectively.

His current research interests include advance control theory, digital signal processors, and their applications in controlling motion systems, electric machine design and control, and power electronics. He is the author of more than 17 papers in control of induction and interior permanent magnet machines, development of various sensorless control algorithms, and interior permanent motor design for traction applications. He also holds six patents in the areas of electric machine and their control.

Dr. Güven is Senior Member of Industry Application Society, since 2001.

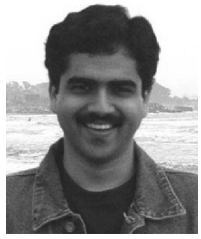

Mahesh S. Illindala (S'01–M'06) received the B.Tech. degree from National Institute of Technology, Calicut, India, in 1995, the M.Sc.(Engg.) degree from Indian Institute of Science, Bangalore, in 1999, and the Ph.D. degree from University of Wisconsin, Madison, in 2005, all in electrical engineering.

Since October 2005, he has been engaged in research, development, and design of power electronics, and electric drive train at Caterpillar Inc., Peoria, IL His current research interests include power electronics, electric drive train, utility applications, and control systems.